Environmental Science and Pollution Research
https://doi.org/10.1007/s11356-022-20022-6

RESEARCH ARTICLE

# Long-term climatology and spatial trends of absorption, scattering, and total aerosol optical depths over East Africa during 2001–2019

Geoffrey W. Khamala[1] · John W. Makokha[1] · Richard Boiyo[2,3] · Kanike Raghavendra Kumar[4]

Received: 29 October 2021 / Accepted: 28 March 2022


## Abstract

The unprecedented increase in anthropogenic activities, coupled with the prevailing climatic conditions, has increased the aerosol load over East Africa (EA). Given this, the present study examined the trends in total, absorption, scattering, and total aerosol extinction optical depth (TAOD, AAOD, SAOD, and TAEOD) over EA, alongside trends in single scattering albedo (SSA). For this purpose, the AOD of different optical properties retrieved from multiple sensors and the Modern-Era Retrospective Analysis for Research and Applications (MERRA-2) model between January 2001 to December 2019 were utilized to estimate trends and assess their statistical significance. The spatial patterns of seasonal mean AOD from the Moderate-resolution Imaging Spectroradiometer (MODIS) sensor and MERRA-2 model were generally characterized with high (>0.35) and low (<0.2) AOD centers over EA observed during the local dry and wet seasons, respectively. Also, the spatial trend analysis revealed a general increase in TAOD, being positive and significant over the arid and semi-arid zones of the northeastern part of EA, which is majorly dominated by locally derived dust. The local dry (wet) months generally experienced positive (negative) trends in TAOD, associated with seasonal cycles of rainfall. High and significant positive trends in AAOD were dominated over the study domain, attributed to an increased amount of biomass burning, variations in soil moisture, and changes in the rainfall pattern. The trends in TAEOD showed a distinct pattern, except over some months that depicted significant increasing trends attributed to changes in climatic conditions and anthropogenic activities. At last, the study domain exhibited decreasing trends in SSA, signifying strong absorption of direct solar radiation resulting in a warming effect. The study revealed patterns of trends in aerosol optical properties and forms the basis for further research in aerosols over EA.

**Keywords** MODIS · OMI · MERRA-2 · AOD · Spatial trends · East Africa

## Introduction

Atmospheric aerosols are tiny-sized particles suspended in the atmosphere with sizes ranging from 0.001 to 100 μm (Seinfeld and Pandis 1998; Tang et al. 2021). Although they comprise a small fraction of the atmosphere, they are among the major climate forcing factors known worldwide (Houghton et al. 2013; Deng et al. 2019; Athar et al. 2021; Guillén-Lambea et al. 2021). They affect climate directly by scattering and absorbing solar radiation, thereby modifying the radiation budget at the top, bottom, and within the atmosphere, which in turn influences the atmospheric heating rate (Charlson et al. 1992; Satheesh et al. 2002). The atmospheric heating rate is strongly dependent on aerosol optical depth (AOD) and single scattering albedo (SSA), being the column-integrated quantities that measure aerosol light extinction and absorption, respectively (Hansen

Kanike Raghavendra Kumar handled the entire review process of the manuscript from submission until its acceptance for publication in the ESPR journal.

Responsible Editor: Gerhard Lammel

✉ Geoffrey W. Khamala
khamalawanjala@gmail.com

[1] Department of Science Technology and Engineering, Kibabii University, P.O. Box 1699-50200, Bungoma, Kenya

[2] Department of Physical Sciences, Meru University of Science and Technology, P.O. Box 972-60200, Meru, Kenya

[3] Department of Environment, Water, Energy and Resources, County Government of Vihiga, Maragoli, Kenya

[4] Department of Physics, Koneru Lakshmaiah Education Foundation (KLEF), Vaddeswaram, Guntur, Andhra Pradesh 522302, India

Published online: 19 April 2022

et al. 1997; Lee et al. 2007). Scattering of incoming solar radiation (by aerosols such as sulfates) results in the cooling of the Earth's atmosphere, whereas absorption by aerosols such as black carbon (BC), mineral dust, and brown carbon (BrC) yields a warming effect. Aerosols alter the optical and microphysical properties of clouds, including their lifetime, formation, and precipitation, and therefore indirectly transform terrestrial radiation (Charlson et al. 1992; Ramanathan et al. 2001).

Because of the aforementioned effects, extensive efforts have been devoted to monitoring atmospheric aerosols using various techniques ranging from in situ and ground-based remote sensing measurements, numerical modeling to satellite-based remote sensing. Although field measurements provide an accurate and detailed description of aerosols, they are usually limited in space and require extensive manpower for constant monitoring and maintenance (Bennouna et al. 2011; Kumar et al. 2014), which eventually results in data gaps. Many ground-based remote sensing networks such as Aerosol Robotic Network (AERONET; Holben et al. 1998), European Aerosol Research Lidar Network (EARLINET; Amiridis et al. 2005), Micro-Pulse Lidar Network (MPLNET; Welton and Campbell 2002), and China Aerosol Remote Sensing Network (CARSNET; Che et al. 2009) procure continuous measurements of aerosol properties in various parts of the globe with very high temporal resolution. However, they require expensive and sophisticated instruments and cover relatively small spatial areas. Recent efforts have also focused on numerical modeling and prediction, which is intended to resolve various atmospheric processes such as sources, transformation processes, transport, and sinks of aerosols and their precursors. This process is usually associated with a large degree of uncertainties related to aerosols processes. Furthermore, they require statistically sophisticated approaches combining observations and models to reduce uncertainties related to the model's initial conditions (Liu et al. 2011).

Given the above constraints, much attention has been devoted to monitoring atmospheric aerosols using several space-borne sensors, which provides an unprecedented opportunity to achieve long-term continuous global characterization of aerosols in terms of spatiotemporal variability and trends. Over the past two decades, several researchers have been working to understand the changes in aerosol optical properties retrieved from multiple satellite sensors such as Advanced Very High Resolution Radiometer (AVHRR; Holben 1986; Ignatov et al. 2004; Akkermans and Clerbaux 2020; Wang et al. 2021), Total Ozone Mapping Spectrometer (TOMS; Prospero et al. 2002; Weber et al. 2018), Multi-angle Imaging SpectroRadiometer (MISR, Kang et al. 2016; Adesina et al. 2016; Boiyo et al. 2018), Ozone Monitoring Instrument (OMI; Torres et al. 2007; Adesina et al. 2016), and MODerate-resolution Imaging Spectroradiometer (MODIS; Remer et al. 2005; Kang et al. 2016; Adesina et al. 2016; Hu et al. 2018; Boiyo et al. 2018).

Using the aforementioned techniques, several studies have been documented to characterize atmospheric aerosols with a special focus on physical, optical, microphysical properties, as well as trends in aerosol properties (Alpert et al. 1998; Mehta et al. 2016; Klingmüller et al. 2016; Hammer et al. 2018; Boiyo et al. 2018; Ramachandran et al. 2020; Jethva et al. 2010; He et al. 2012, 2016; Kang et al. 2014; Adesina et al. 2016; Boiyo et al. 2019, 2018; Kumar et al. 2014, 2015; Aklesso et al. 2018; Khan et al. 2021, 2020). For example, Mehta et al. (2016) reported increasing trends in various regions of the world attributed to increasing anthropogenic activities, whereas other regions recorded decreasing trends resulting from strict implementation of environmental regulations. In some parts of the globe, such as Europe and North America, Li et al. (2014) reported a decrease in total aerosol optical depth (TAOD) attributed to emission control measures as well as changes in the local aerosol source. Using combined Dark Target/Deep Blue AOD, Klingmüller et al. (2016) reported a positive trend in most parts of the Middle East associated with increased long-distant transport of aerosols by the surface wind. The study further attributes positive AOD trends to negative trends in the soil moisture content that translates into enhanced dust emissions emanating from enhanced anthropogenic influence. Kumar et al. (2014) examined the seasonal and inter-annual variability of AOD over Cape Town, Bloemfontein, and Durban in South Africa. Except for spring, they reported a decreasing trend in the annual and seasonal mean AOD, attributed to the implementation of policies geared toward pollution control.

The linear trend analysis and spatiotemporal heterogeneity in MODIS AOD studied by Aklesso et al. (2018) over three countries in Southern West Africa revealed decreasing trends in most regions of the study domains, with increasing trends specifically noted over highly urbanized and densely populated areas in the southern coastal parts. The negative trends were associated with a reduction in dust and sea salt aerosols, whereas positive trends were attributed to an increase in anthropogenic activities. Over East Africa (EA), Makokha et al. (2017) determined long-term annual and seasonal trends in total AOD at 550 nm and reported significant seasonality in AOD. On AOD trends, their study indicated a decreasing trend over most of the parts of Kenya except Nairobi, where they observed an increasing trend. The study further attributed positive trends over Nairobi to increasing population, industrial-vehicular emission, and biomass burning, whereas negative trends were attributed to washout and/or dynamics played by the local meteorology. On the other hand, studies by Boiyo et al. (2018) over EA revealed the dominance of positive AOD trends associated with increased anthropogenic activities.

East Africa, hereafter simply represented as EA, is one of the regions around the globe that requires extensive characterization of aerosols in terms of microphysical, optical, and radiative properties, as well as spatiotemporal distribution, trends, and associated properties. The region is currently experiencing an unprecedented increase in aerosol concentration attributed to changes in anthropogenic activities, emission sources, and prevailing meteorological conditions (Makokha et al. 2017; Boiyo et al. 2018). The proximity of the region to the Indian Ocean, the Sahara Desert, and central Africa's Democratic Republic of Congo (DRC) basin makes it susceptible to distinct aerosol types (Makokha and Angeyo 2013; Boiyo et al. 2017). Despite this, the region lags behind the rest of the world on matters related to atmospheric aerosols. Previous investigations over the region documented the existence of fine- and coarse-mode aerosols from various natural and anthropogenic sources, resulting in varying concentrations at different spatiotemporal scales (de Graaf et al. 2010; Makokha et al. 2018; Boiyo et al. 2019). However, delineation of trends based on aerosol characteristics, which bears a decisive role in evaluating aerosol-climatic impact (including the aerosol radiative forcing, ARF), is largely missing over the region. This has not only hindered detailed investigation of aerosol optical properties but also hampered the region's ability to precisely quantify the climatic effects of atmospheric aerosols. Therefore, improved and continued characterization of aerosols in terms of trends in total, absorption, scattering, and total aerosol extinction optical depths is largely required over East Africa.

Keeping in mind of the aforementioned demand, the present study complements previous works (e.g., Ngaina and Muthama 2014; Makokha et al. 2017; Boiyo et al. 2017, 2018) over the region by investigating trends in total (TAOD), absorption (AAOD), scattering (SAOD), and total aerosol extinction optical depths (TAEOD) as well as trends in SSA over East Africa. The study seeks to answer the question in the context: "what pattern do aerosol properties define over EA." In doing so, the study assesses distinctively the trends in TAOD, AAOD, SAOD, TAEOD, and SSA in a view to examine the cause of the overall changes in AOD. The rest of this paper is structured as follows: the study area and meteorology section illustrate the study area, data, and methodology. Results and discussions are documented in the results and discussion section, while the summary and conclusions section summarizes the key findings drawn from the present work.

## Study area and meteorology

The study was conducted over East Africa (EA), a region that is bounded by latitudes 12° S–5° N and longitudes 28° E–42° E; with Kenya, Uganda, and Tanzania being the three constituent countries (Fig. 1). The domain is bounded by Ethiopia and Sudan to the north, Somalia and the Indian Ocean to the east, Rwanda, Burundi, and DRC to the west, and Mozambique and Zambia to the south. The domain has a multilayered topography that ranges from the glaciated mountain, plateaus, and the coastal plain with an altitude ranging from sea level to the highest altitude of 5895 m (Mt Kilimanjaro) (Ngaina and Muthama 2014). Additionally, EA experiences a tropical climate influenced by several factors such as Intertropical Convergence Zone (ITCZ), El Nino-Southern Oscillation (ENSO), and Indian Ocean Dipole (IOD) (Ongoma and Chen 2017; Boiyo et al. 2018). Based on prevailing meteorological conditions, a year has been divided into four seasons. January–February (JF) and June–July–August–September (JJAS) represent the local dry seasons, characterized by reduced rainfall and increased aerosol load. On the other hand, March–April–May (MAM) and October–November–December (OND) represent the local wet seasons, characterized by enhanced rainfall and reduced aerosol concentrations (Ayugi et al. 2016, 2020; Nicholson 2017; Gebrechorkos et al. 2019; Caroline et al. 2021). More details concerning the dynamics played by meteorology over the study domain have been investigated by Boiyo et al. (2018).

## Instrumentation and data

### The MODIS sensor

The MODIS sensor was launched into the Earth's orbit, with daytime equator crossing at 10:30 h local time (LT = UTC + 3h), by the National Aeronautics and Space Administration (NASA) Goddard Space Flight Center (GSFC) on 18th, December 1999 onboard the Terra satellite. The second was launched on May 4, 2002, onboard the Aqua platform (Remer et al. 2005) and has a daytime equator crossing at 13:30 h LT. The sensor has a swath of ~2330 km, with a temporal resolution of 1–2 days, and acquires data over 36 spectral bands ranging in wavelengths from 0.415 to 14.235 μm at three spatial resolutions (2 bands at 250 m, 5 bands at 500 m, and 29 bands at 1 km). Seven of these bands operating in near-ultraviolet (UV), visible and near-infrared spectroscopy (IR) wavelength regions (0.415–2.155 μm) can effectively retrieve AOD over land and ocean (Hsu et al. 2013; Sayer et al. 2013, 2014) using two different algorithms: "Dark Target (DT)" and "Deep Blue (DB)" (Floutsi et al. 2016).

MODIS aerosol products are stored at different levels and under various versions called "collections." The MODIS data processing levels include level 1.0 (geolocated radiance and brightness temperature), level 2.0 (retrieved geophysical data products), and level 3.0 (gridded points). MODIS retrieval accuracy over land and ocean (Tanre et al. 1997;

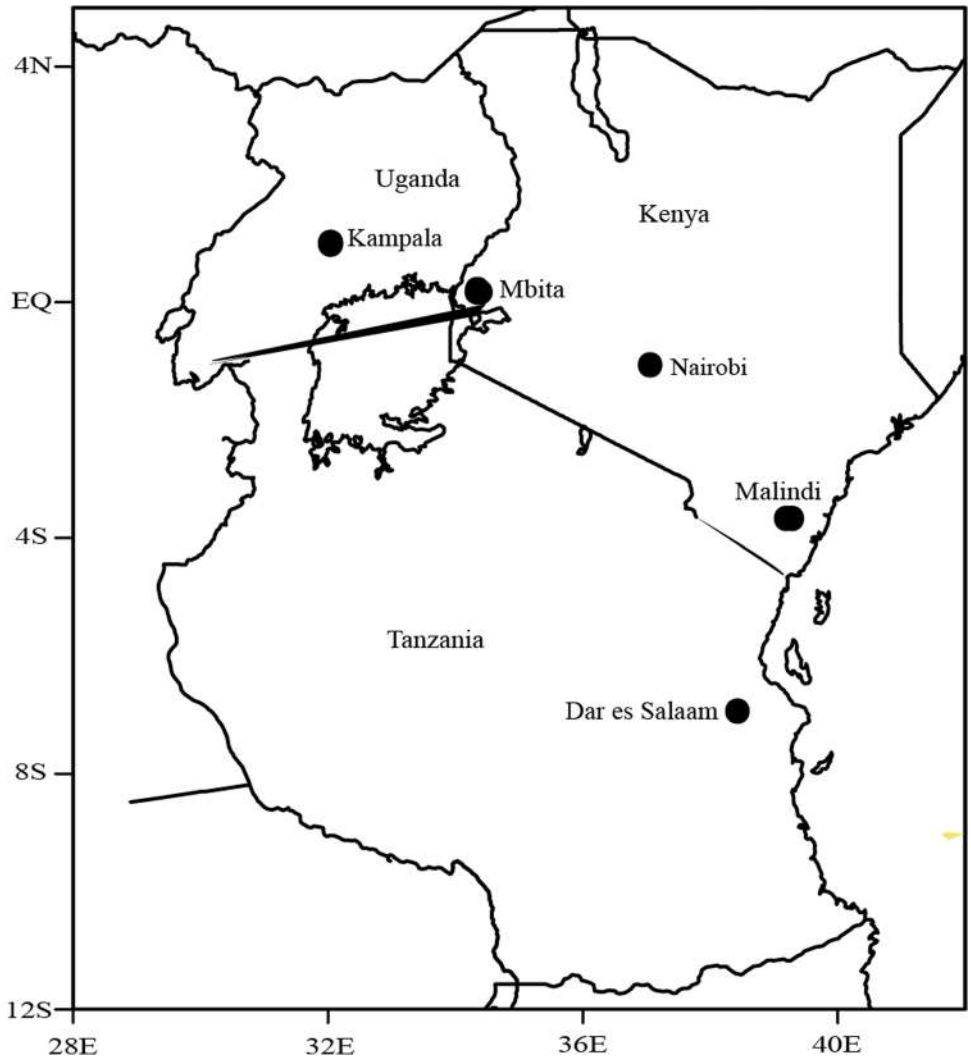


**Fig. 1** Study region showing East Africa and its constituent countries

Remer et al. 2005) was estimated to be ±0.05 ± 0.20 (AOD) and ±0.03 ± 0.15 (AOD), respectively, for level 2 products. Detailed information concerning the sensor, data products, retrieval algorithms, calibration, and uncertainties can be found elsewhere (Hsu et al. 2004, 2013; Levy et al. 2010; Sayer et al. 2013, 2014). The present study utilized Collection 6.1 (C006.1), level 3 monthly $TAOD_{550}$ retrieved from MODIS Terra (combined DTB) at a spatial resolution of 1° × 1° for a period of 18 years (January 2001 to December 2019) to study trends and their significance levels over EA. These data products were sourced from http://giovanni.gsfc.nasa.gov/giovanni/.

### The OMI sensor

The OMI is a hyper-spectral passive satellite with a wavelength range of 270–500 nm. It was launched in July 2004 by NASA's Earth Observing System (EOS) onboard the Aura satellite by the Netherlands Agency for Aerospace Programs in collaboration with the Finnish Meteorological Institute (Levelt et al. 2006; Torres et al. 2007). Although initially designed to retrieve data of trace gases, OMI's wavelength range of ~400 nm allows detection of elevated layers of absorbing aerosols hence providing valuable information on the aerosol type of a particular region at four processing levels: level 0, level 1B, level 2, and level 3. The OMI uses a nadir-viewing imaging spectrometer to measure the top of the atmosphere (TOA) upwelling radiances in the ultraviolet and visible regions of the solar spectrum (270 to 500 nm) at a spatial resolution of approximately 0.5 nm (Livingston et al. 2009). OMI uses two algorithms for retrieving aerosol information from OMI measurements of TOA reflectance: the OMAERUV aerosol product (near-UV algorithm) and the OMAERO aerosol product (multi-wavelength algorithm) (Torres et al. 2007). By employing the OMAERUV algorithm, OMI provides aerosol parameters such as aerosol absorption optical depth (AAOD), single scattering albedo (SSA), and absorbing aerosol index (Torres et al.

2005, 2007). More details concerning OMI's data products, retrieval algorithms, calibration, and uncertainties have been described by several authors, including Torres et al. (1998, 2007), Adesina et al. (2016), Boiyo et al. (2017), and Kumar et al. (2017). To examine trends in absorbing aerosols (such as black carbon and dust) and single scattering albedo, the AAOD and SSA at 500 nm from OMI ($AAOD_{500}$ and $SSA_{500}$) are derived at a spatial resolution of 1° × 1° for a period of 15 years (January 2005 to December 2019). The data (sourced from http://giovanni.gsfc.nasa.gov/giovanni/) were used because the product is known for its high reliability (Torres et al. 2007; Livingston et al. 2009).

#### The MERRA-2 model

The MERRA-2 is a global atmospheric reanalysis data launched by the NASA Global Modeling and Assimilation Office (GMAO) in 2009 (Rienecker et al. 2011). The model is based on the version of the GEOS-5 atmospheric data from 1980 to 2016 at 0.5° × 0.625° resolution with 72 layers and spanning the satellite observing era from 1980 to the present (Wu et al. 2002; Rienecker et al. 2011; Khan et al. 2021). The initial MERRA model has been improved in terms of analysis, forecasting, data assimilation as well as bias correction of aircraft observation to the MERRA-2 model in 2017 (Gelaro et al. 2017). This model performs meteorological data assimilation, aerosols analysis, precipitation, water vapor climatology, and temperature using NASA's observations of stratospheric ozone. Building on the success of the atmospheric reanalysis conducted with GEOS, the current improvements in the MERRA-2 model intend at producing a major Earth System Reanalysis of the atmosphere, land, ocean, and ice at a latitude-longitude grid. In the present study, MERRA-2 M2TMNXAER v5.12.4 level-3 monthly time-averaged data for $SAOD_{550}$ and total aerosol extinction optical depth (M2TMNXAER_5_12_4_TOTEXTTAU) were retrieved for the analysis of trends in scattering aerosols and total aerosol extinction (total absorption and scattering per unit atmospheric depth) ($TAEOD_{550}$) at a spatial resolution of 0.5° × 0.625° from January 2001 to December 2019. These data products were sourced from ttp://giovanni.gsfc.nasa.gov/giovanni/.

### Trend analysis

Several statistical approaches exist to quantify trends in the time series of a geophysical variable. In the present work, linear regression analysis was used to estimate monthly trends in TAOD, SAOD, and AAOD alongside trends in key aerosol parameters (TAEOD and SSA). The method has been discussed extensively by Weatherhead et al. (1998) and used in many related studies (Kumar et al. 2014, 2015; Kang et al. 2016; Adesina et al. 2016; Dahutia et al. 2017). Following this method, a linear trend model (Eq. 2.1) was adopted as

$$Y_t = c + \omega^* X_t + \varepsilon \tag{2.1}$$

where $Y_t$ is the geophysical variable for which the trend is being estimated, $c$ is the offset ($y$-intercept) which represents the value of $Y_t$ at the beginning of the time series, $X_t$ is the independent variable representing time, ω is the trend estimate of the geophysical variable, whereas ε is the noise in the time series.

The statistical significance of the estimated trends was further tested using the method developed by Weatherhead et al. (1998). In this regard, trends are considered significant at a $p$-value of 0.05 or 95% confidence when $\left|\frac{\omega}{\delta}\right| > 2$, whereas trends are considered significant at a 90% confidence when $1.5 < \left|\frac{\omega}{\delta}\right| < 2$; where δ is the standard deviation of the slope obtained from the linear regression. This method has the practical advantage of simply assessing the direction and magnitude of variations in long-term data (e.g., Zhang and Reid 2010; Kumar et al. 2014, 2015; He et al. 2016; Mehta et al. 2016; Kang et al. 2016; Dahutia et al. 2017) and was therefore considered suitable for executing pixel-wise and domain averaged analysis.

## Results and discussion

### Seasonal distribution of AOD

AOD constitutes an important parameter of atmospheric aerosols and could be used to quantify columnar aerosol burden in the atmosphere (Luo et al. 2014; Kumar et al. 2015). The climatological patterns of seasonal mean AOD derived from MERRA-2 and MODIS Terra (combined product) over EA during the study period are shown in Fig. 2. The spatial patterns of seasonal mean aerosol loading were generally characterized by low, moderate, and high AOD indicating distinct characteristics of the aerosol load. Low (<0.2) AOD centers were specifically observed by both sensors in highly vegetated areas with relatively high altitudes and more rainfall over western and central parts of Kenya and central and southeastern parts of Tanzania. While moderate to high (>0.35) AOD values were observed over arid and semi-arid areas of eastern and northern parts of Kenya and the coastal region. This could be attributed to the long-range transport of dust by the north easterlies together with those locally generated from the ocean, respectively (Gatebe et al. 2001; Ngaina and Muthama 2014).

In terms of area coverage and strength, the regional aerosol load from both the MODIS sensor and MERRA-2 model was found high during JJAS, followed by JF and OND, and

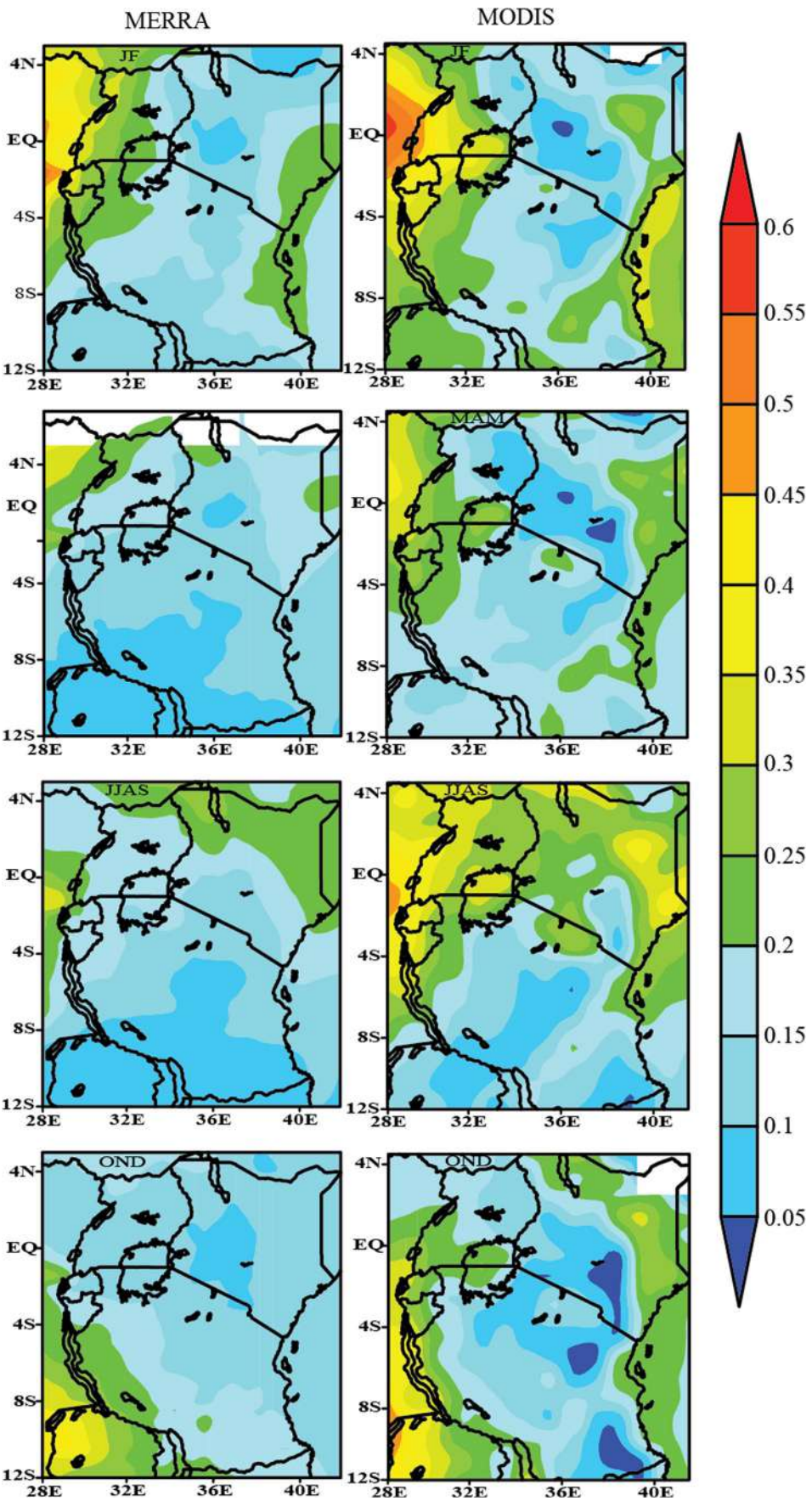


**Fig. 2** Spatial climatology of seasonal mean AOD derived from the MERRA-2 and MODIS-Combined (DTB) for different seasons over EA from 2001 to 2019

minimum during MAM. During the local dry seasons, high AOD values were noted over the dust dominant zones of northwest and northeast Kenya, as well as the southwest parts of Uganda and Tanzania. On the other hand, very low AOD values (<0.1) were characterized during the local wet seasons over high rainfall areas of western and central parts of Kenya, northeast Uganda, and southwest Tanzania. The seasonal patterns of AOD over EA are closely associated with the seasonal cycle of rainfall, with the two depicting a relatively inverse relationship (de Graaf et al. 2010; Ayugi et al. 2020; Caroline et al. 2021). The enhanced rainfall during MAM causes large wet deposition and suppresses the emission of aerosols from the ground. Conversely, the enhanced aerosol loading during the local dry seasons could be attributed to increased anthropogenic activities that release a significant amount of aerosols into the atmosphere (Ngaina and Muthama 2014; Makokha et al. 2017; Boiyo et al. 2018).

## Trends in total aerosol optical depth

Figure 3 depicts spatial trends in columnar TAOD and their statistical significance over EA in all the months during the study period. The trends are estimated in terms of increase/decrease and indicated by positive/negative values. In general, positive trends in TAOD were found higher (0.002 year$^{-1}$) and significant at a 90% confidence level over the arid and semi-arid areas of the northeast part of the study domain dominated by dust. The increased positive trends over the northeast part of the study domain could be attributed to reduced rainfall that increases locally generated dust (Boiyo et al. 2018). Significantly positive trends dominate the local dry months (June, July, August, and September), signifying increased aerosol production due to reduced wet deposition and increased anthropogenic activities such as biomass burning. Additionally, the strongest increasing trends along with the coastal and western parts of EA were recorded in January with a magnitude of >0.0004 year$^{-1}$. This could be attributable to increased anthropogenic activities (land preparation and biomass burning) as well as reduced rainfall (Boiyo et al. 2018; Ngaina and Muthama 2014; Makokha et al. 2017). On the other hand, negative trends dominate the local wet months (March, April, May, and October), which is pronounced and significant during May over the northwest, west, and southwest areas of EA. The negative trends during these months could be attributed to the large wet deposition of aerosols resulting from the seasonal cycles of rainfall over the study domain (De Graaf et al. 2010; Makokha et al. 2017).

The observed positive trends in TAOD in most parts of EA interpret as an increase in aerosol load. However, the magnitudes and signs are influenced by both emission and meteorological factors. EA is experiencing an overall increase in temperature and reduced rainfall, conditions favorable for increased aerosol emissions (Boiyo et al. 2019). The positive trends over the arid and semi-arid regions in the northeast of the study domain, as well as those observed during the local dry months, could be associated with reduced rainfall, increasing locally generated dust

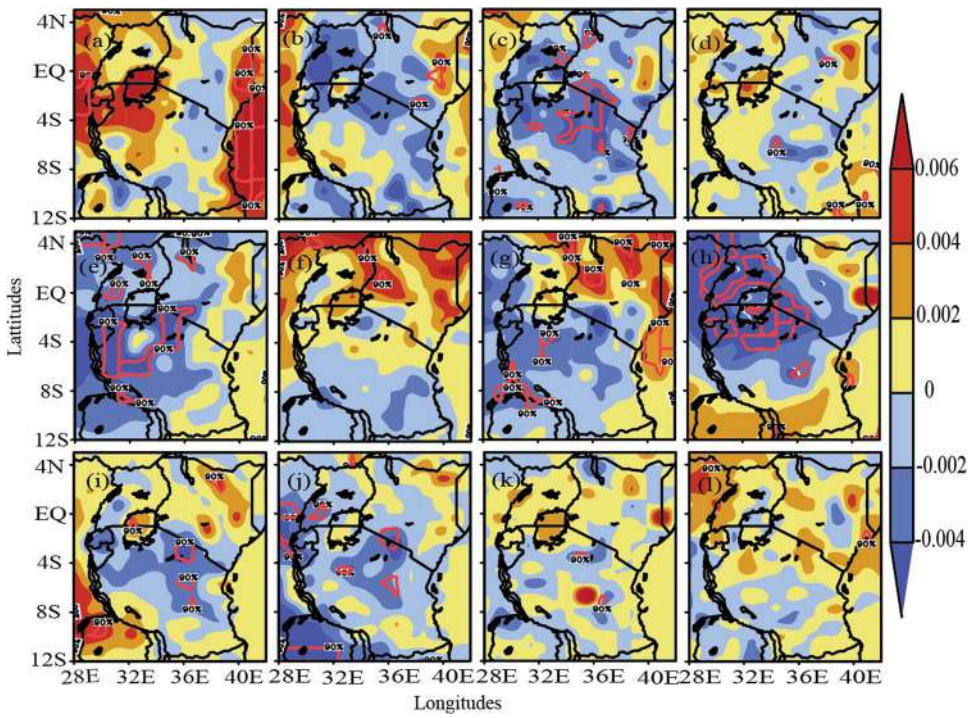


**Fig. 3** **a–l** Spatial patterns of annual mean trends (in the units of year$^{-1}$) in TAOD from January to December from 2001 to 2019. The shadings show the sign and magnitude of the trend, while the confidence levels are labeled in all the panels

(Boiyo et al. 2018). On the other hand, the positive trends observed in the border regions with DRC during specific months of the year could be attributed to intense biomass burning activities (de Graaf et al. 2010). In addition, the local anthropogenic activities arising from increased biomass burning and industrial-vehicular emissions (Kinney et al. 2011; Makokha and Angeyo 2013; Ngo et al. 2015) could contribute to the observed positive trends in TAOD. Conversely, the negative trends in TAOD over the local wet months interpret as a reduced aerosol load associated with increased wet deposition from the seasonal cycles of the rainfall over the study domain.

## Trends in absorption aerosol optical depth

Figure 4 shows the trends in AAOD during 2005–2019 over EA, with an increase/decrease being depicted by positive/negative values. Generally, EA is dominated by positive trends in AAOD, being high and significant (at 90% confidence level) in most months except March, with enhanced rainfall. The trends of AAOD followed a similar pattern as that of total TAOD, indicating the dominance of absorbing aerosols in TAOD over EA. The observed positive trends in AAOD could be attributed to increased biomass burning that characterizes the tropical atmospheric conditions over EA, coupled with prevailing meteorological conditions (Boiyo et al. 2018, 2019). Notably, the significantly increasing trends in AAOD in January (0.006 year$^{-1}$) could be attributed to increased biomass burning, variations in soil moisture, increasing dust loading, and changes in the rainfall pattern over the study domain. The similarity in trends between TAOD and AAOD implies that an increase in TAOD over EA is largely contributed by absorbing aerosols, evidenced by the high values of AAOD. Notably, some areas of the study domain exhibited negative trends in AAOD; being dominant over the coastal parts of the study domain, the Indian Ocean, and northeast of the study domain. The decreasing trend in AAOD in these areas could be attributed to reduced biomass burning and changes in land-use patterns. In March, the significant decline in AAOD observed over EA is attributed to increased rainfall, accompanied by reduced biomass burning and suppressed dust emission.

## Trends in scattering aerosol optical depth

Scattering aerosol optical depths are computed by subtracting absorption aerosol optical depth from total aerosol optical depth. Figure 5 shows trends in SAOD in all the months from 2001 to 2019 over EA, with an increase/decrease in SAOD portrayed by positive/negative trends (Prijith et al. 2017). The negative trends dominate the study domain, being higher (0.004 year$^{-1}$) and significant at a 90% confidence level over the western region of the study domain. Significantly negative trends (>0.004 year$^{-1}$) were noticed in May and December over the coastal, west, and northwest regions of the study area. The negative trends in SAOD over the observed region and on the specific month could be

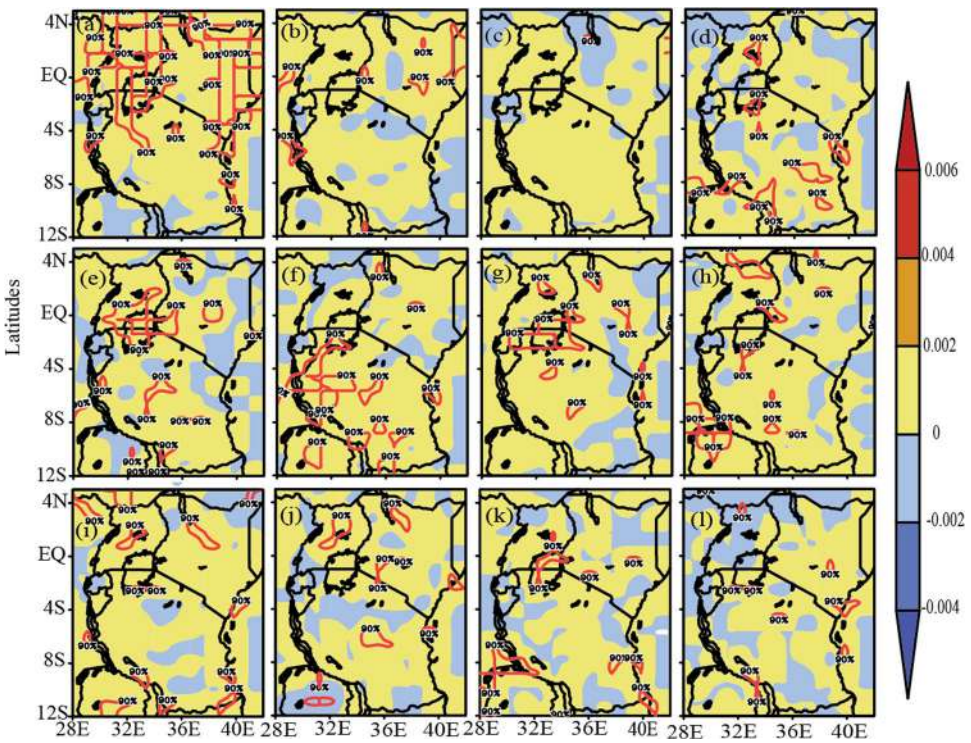


**Fig. 4** Same as in Figure 3, but for AAOD

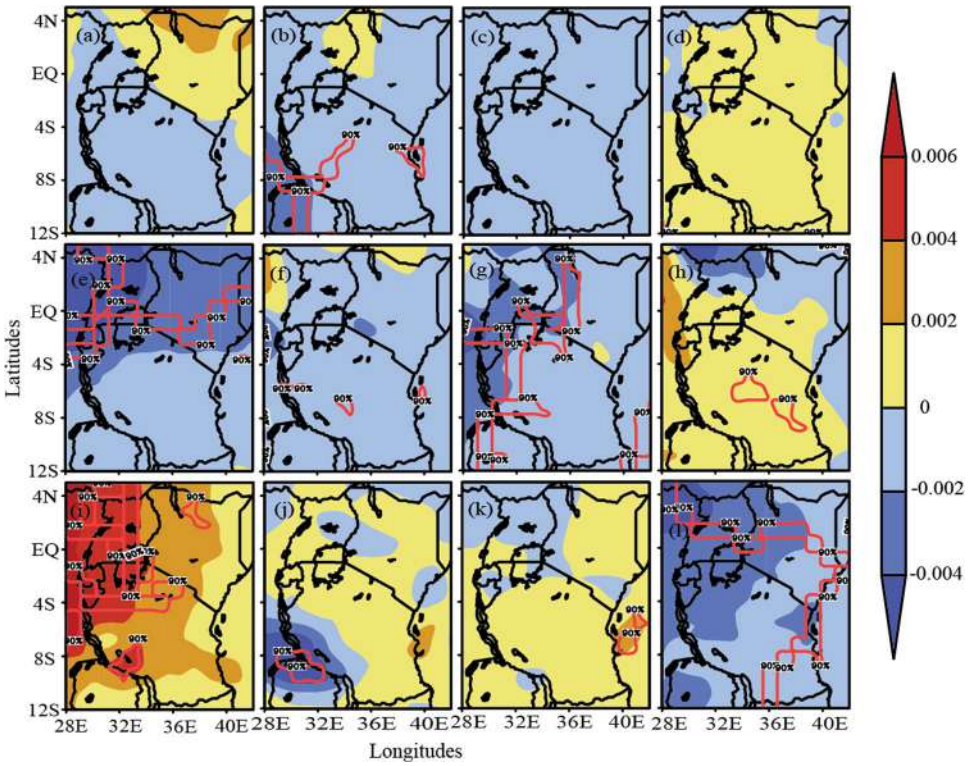


**Fig. 5** Same as in Figure 3, but for SAOD

attributed to enhanced precipitation which suppresses the dust aerosols over the region.

On the other hand, positive trends are observed in specific months of the year, being dominant during January, April, August, September, and November. The trends in SAOD over these months follow a similar pattern as that of TAOD, indicating the dominance of scattering aerosols in TAOD during these specific months. This could be attributed to prevailing climatic conditions, characterized by reduced rainfall leading to enhanced generation of dust aerosols.

## Trends in total aerosol extinction optical depth

The implications of the depicted trends in AAOD, SAOD, and TAOD were determined by evaluating trends in TAEOD (sum of AAOD and SAOD; Fig. 6). The trends in TAEOD (representing the total effect of radiation passing through the medium) experienced significant heterogeneity, being significantly negative during some months (February, May, June, July, and December) and significantly positive during April, August, and September. The significantly negative trends in TAEOD (Table 1 and Fig. 5) interpret reduction in the scattering of light radiation, attributed to enhanced rainfall, which suppresses dust emission resulting in reduced SAOD. On the other hand, the observed significant positive trends in TAEOD, especially in September (~0.0018 year$^{-1}$), could be attributed to reduced rainfall resulting in to increase in dust loading that enhances the emission of sulfates, nitrates, and organic aerosols into the atmosphere (Pathak and Kumar 2014)

## Trends in single scattering albedo

The SSA is a vital intensive parameter that controls the magnitude and sign of aerosol radiative forcing (ARF). For example, a small change in SSA from ~0.9 to ~0.8 (~11% decrease) can often change the sign of ARF from negative (cooling) to positive (warming), depending on the reflectance of the underlying surface and altitude of the aerosols (Jethva et al. 2010). EA predominantly exhibits a significantly decreasing trend in SSA (Fig. 7), implying strong absorption of direct solar radiation and reflected radiation caused by bright surfaces, causing an overall warming effect. This is attributed to an increase in absorbing aerosols, mainly from biomass burning and industrial-vehicular emissions. Notably, biomass burning emits not only OC and Sulfate aerosols but also BC, which could result in significant negative trends in SSA.

However, positive trends in SSA dot some parts of the study domain, being predominant over the Northeast of the study domain. This interprets to increase in SSA (to higher values) attributed to the dominance of non-absorbing aerosols (mainly sulfate) emanating from the dust-stricken areas of the domain. Also, positive trends in SSA are observed over the Indian Ocean, likely associated with non-absorbing sea-salt aerosols.

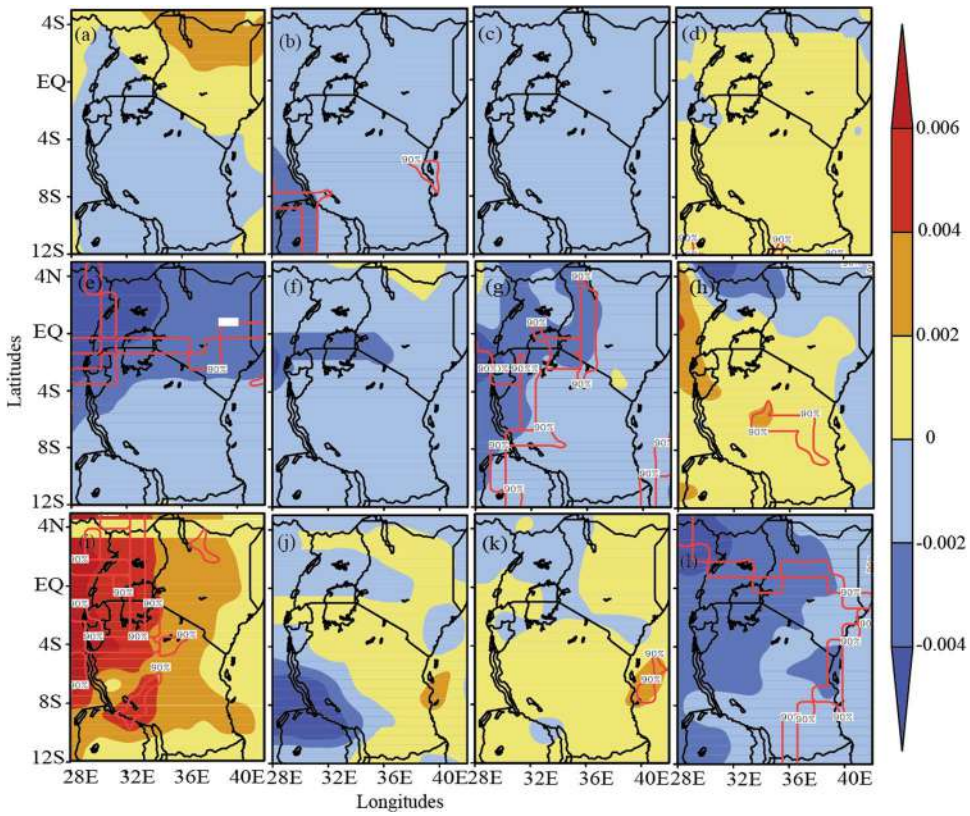


**Fig. 6** Same as in Figure 3, but for TAEOD

**Table 1** Mean trends of the total, absorbing, and scattering aerosol optical depths observed in different countries over East Africa

| Month | TAOD ($year^{-1}$) (January 2001–December 2019) | | | | AAOD ($year^{-1}$) (January 2005–December 2019) | | | | SAOD ($year^{-1}$) (January 2001–December 2019) | | | |
|---|---|---|---|---|---|---|---|---|---|---|---|---|
| | KE | TZ | UG | EA | KE | TZ | UG | EA | KE | TZ | UG | EA |
| January | 0.0010 | 0.0022 | 0.0013 | 0.0018 | 0.0005 | 0.0007 | 0.0008 | 0.0006 | 0.0025 | 0.0050 | 0.0038 | 0.0041 |
| February | −0.0006 | −0.0016 | −0.0024 | −0.0014 | 0.0004 | 0.0004 | 0.0003 | 0.0003 | −0.0008 | −0.0001 | 0.0010 | −0.0005 |
| March | −0.0011 | −0.0022 | −0.0016 | −0.0015 | 0.0003 | 0.0003 | 0.0003 | 0.0003 | −0.0016 | −0.0017 | −0.0021 | −0.0016 |
| April | 0.0002 | 0.0007 | 0.0007 | 0.0005 | 0.0002 | 0.0002 | 0.0002 | 0.0002 | −0.0008 | 0.0002 | −0.0011 | −0.0004 |
| May | −0.0003 | −0.0017 | −0.0014 | −0.0010 | 0.0002 | 0.0002 | 0.0002 | 0.0002 | 0.0000 | −0.0008 | −0.0006 | −0.0003 |
| June | 0.0032 | 0.0003 | 0.0030 | 0.0018 | 0.0002 | 0.0003 | 0.0001 | 0.0002 | 0.0014 | −0.0016 | 0.0023 | 0.0000 |
| July | 0.0023 | −0.0004 | 0.0015 | 0.0011 | 0.0003 | 0.0001 | 0.0004 | 0.0002 | −0.0003 | −0.0033 | −0.0015 | −0.0015 |
| August | 0.0045 | −0.0004 | 0.0028 | 0.0003 | 0.0002 | 0.0003 | 0.0003 | 0.0003 | −0.0012 | −0.0019 | −0.0015 | −0.0014 |
| September | 0.0012 | −0.0001 | 0.0008 | 0.0005 | 0.0002 | 0.0002 | 0.0003 | 0.0002 | −0.0020 | −0.0028 | −0.0014 | −0.0021 |
| October | −0.0002 | −0.0006 | −0.0008 | −0.0005 | 0.0003 | 0.0003 | 0.0004 | 0.0002 | −0.0001 | 0.0026 | 0.0001 | 0.0014 |
| November | 0.0004 | 0.0006 | 0.0015 | 0.0006 | 0.0002 | 0.0004 | 0.0001 | 0.0003 | −0.0003 | 0.0000 | −0.0002 | −0.0001 |
| December | 0.0008 | 0.0001 | 0.0019 | 0.0005 | 0.0001 | 0.0002 | −0.0001 | 0.0001 | −0.0007 | −0.0007 | −0.0009 | −0.0008 |

*TAOD*, total aerosol optical depth; *AAOD*, absorption aerosol optical depth; *SAOD*, scattering optical depth; *KE*, Kenya; *TZ*, Tanzania; *UG*, Uganda; *EA*, East Africa

## Mean trends analysis

The monthly mean trends in TAOD, AAOD, and SAOD over specific countries of the study domain (Kenya, Uganda, and Tanzania) and the entire EA were assessed and tabulated (Table 1). The mean trend in TAOD and SAOD over each of the individual countries and entire EA was found to be generally negative during local wet months, attributed to seasonal cycles of rainfall and anthropogenic activities. On the other hand, East Africa and each of the constituting countries were dominated by positive trends in TAOD, being enhanced (~0.0018 $year^{-1}$)

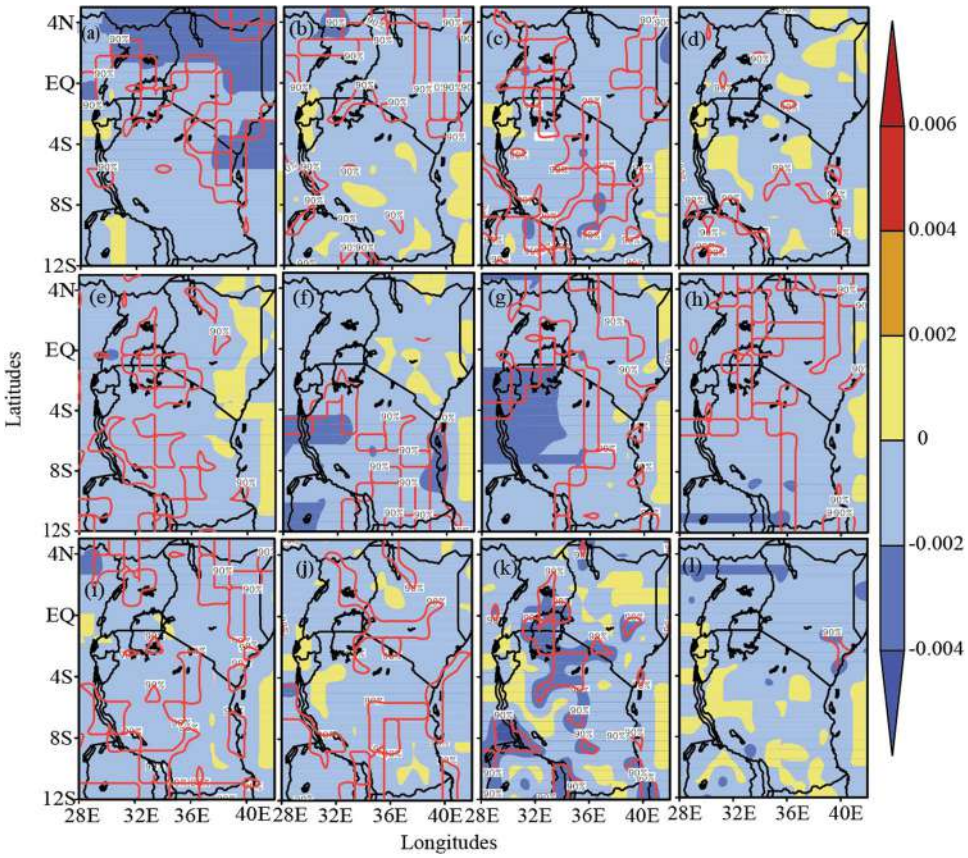


**Fig. 7** Same as in Figure 3, but for SSA

over Kenya and Uganda, resulting in an overall positive trend (Table 1). As previously mentioned, the enhanced positive trends in TAOD during the local dry seasons are consistent with the seasonal cycles of emission sources and modulations induced by the local meteorology (Boiyo et al. 2018).

The study domain was further characterized by positive trends in AAOD in all months, with the highest (lowest) values of (~0.006 year$^{-1}$) (0.0001 year$^{-1}$) observed in January (December), attributed to changes in climatic conditions and anthropogenic activities (Section 3.3). However, negative trends in SAOD dominated the study domain, being pronounced in September (~0.0021 year$^{-1}$) and August (~0.0014year$^{-1}$), with positive trends observed in January and October; all associated with the seasonal cycles of rainfall. The mean trend in TAEOD (Table 2) was dominated by negative trends except for some months (January, April, June, September, and November) that exhibited positive trends attributed to modulations induced by prevailing climatic conditions on the emission sources. On the other hand, negative trends in SSA characterized the study domain in all months, being pronounced during the dry months of January (~ − 0.0017 year$^{-1}$), June (~ − 0.0014 year$^{-1}$), and July (~−0.0013 year$^{-1}$). This indicates increased absorbing aerosols from anthropogenic activities.

## Summary and conclusions

Using multi-years of level-3 aerosol data sets retrieved from the MODIS and OMI sensors and the MERRA-2 model, the present study revealed an in-depth understanding of trends in TAOD, AAOD, SAOD, TAEOD, and SSA, as well as spatial distribution in TAOD over EA for the period 2001–2019. The spatial patterns of seasonal mean AOD from the MODIS sensor and MERRA-2 model were generally characterized by low (<0.2), moderate (0.2–0.35), and high (>0.35) centers over EA. Low AOD was observed over highly vegetated areas with relatively high altitude and rainfall over western and central parts of Kenya, and central and southeastern parts of Tanzania, whereas moderate to high AOD characterized the arid and semi-arid areas of eastern and northern parts of Kenya and the coastal region. The seasonal aerosol load was low (high) during the local wet (dry) season, attributed to the prevailing climatic conditions.

Trends in TAOD depicted a general increase, being high and significant over the northeastern part of the study domain, whereas the local wet (dry) month exhibited a general decrease (increase) in aerosol load. The study domain was dominated by positive trends in AAOD, being high and significant (at 90% confidence level) in most of the months, except March, with

**Table 2** Mean trends of total aerosol extinction optical depth (TAEOD) and single scattering albedo (SSA) over EA

| Months | TAEOD ($year^{-1}$) (January 2001–December 2019) | | | | SSA ($year^{-1}$) (January 2005–December 2019) | | | |
|---|---|---|---|---|---|---|---|---|
| | KE | TZ | UG | EA | KE | TZ | UG | EA |
| January | 0.0004 | 0.0015 | 0.0006 | 0.0010 | −0.0017 | −0.0012 | −0.0018 | −0.0017 |
| February | −0.0008 | −0.0005 | −0.0010 | −0.0005 | −0.0011 | −0.0010 | −0.0010 | −0.0011 |
| March | −0.0015 | −0.0008 | −0.0011 | −0.0008 | −0.0010 | −0.0012 | −0.0012 | −0.0010 |
| April | 0.0001 | 0.0001 | 0.0008 | 0.0003 | −0.0006 | −0.0007 | −0.0008 | −0.0007 |
| May | −0.0021 | −0.0024 | −0.0014 | −0.0022 | −0.0006 | −0.0010 | −0.0006 | −0.0009 |
| June | 0.0014 | −0.0006 | 0.0027 | 0.0008 | −0.0006 | −0.0015 | −0.0002 | −0.0014 |
| July | 0.0006 | −0.0014 | 0.0012 | −0.0003 | −0.0010 | −0.0013 | −0.0012 | −0.0013 |
| August | −0.0021 | −0.0007 | −0.0039 | −0.0013 | −0.0010 | −0.0012 | −0.0011 | −0.0012 |
| September | 0.0003 | 0.0022 | 0.0018 | 0.0018 | −0.0010 | −0.0010 | −0.0010 | −0.0010 |
| October | −0.0006 | 0.0003 | −0.0006 | −0.0003 | −0.0006 | −0.0008 | −0.0008 | −0.0008 |
| November | 0.0004 | 0.0007 | 0.0002 | 0.0005 | −0.0010 | −0.0012 | −0.0007 | −0.0010 |
| December | 0.0004 | −0.0013 | −0.0004 | −0.0006 | −0.0008 | −0.0005 | −0.0004 | −0.0007 |

declining AAOD. The increase in trends in AAOD is attributed to increased biomass burning, variations in soil moisture resulting in an increase of dust loading, and changes in the rainfall pattern over the study domain.

The study domain was dominated by negative trends in SAOD, except for specific months that depicted positive trends. The dominance in negative trends was attributed to enhanced rainfall, which suppressed the emission of dust aerosols over the study domain, whereas the positive trends in SAOD (which contributed significantly to TAOD) were attributed to reduced rainfall resulting in dust emission. Seasonally, positive trends in TAOD were observed during the local dry seasons (JJAS and JF), whereas negative trends in TAOD dominated the local wet seasons (MAM and OND), attributed to changes in climatic conditions and anthropogenic activities. Positive trends in AAOD dominated the study domain, whereas negative trends in SAOD characterized the study domain. The trends in TAEOD showed a distinct pattern, being dominated by significantly decreasing trends during February, May, June, July, and December attributed to wet deposition. The significantly increasing trends in TAEOD were observed during April, August, and September, attributed to anthropogenic factors such as biomass burning and industrial-vehicular emissions. Reduced rainfall resulted in dust emissions. The study domain significantly exhibited a decreasing trend in SSA in all the months, attributed to the presence of absorbing aerosols from biomass burning that characterize the tropical region and motor-vehicular emissions, which caused a warming effect.

A delineation of aerosol optical properties such as TAOD, AAOD, SAOD, and TAEOD, in addition to the spatial trends determined, would comprehensively quantify aerosol effects on climate, air quality, and human health as well as aerosol direct radiative forcing that are majorly lacking over EA, hence need for further investigation.

**Acknowledgements** The authors are thankful to the NASA LAADS and Giovanni online analysis and visualization system for providing and processing MODIS, MERRA-2, and OMI satellite data used in this study. The lead author (Mr. Geoffrey W. Khamala) extends sincere gratitude to the Ministry of Higher Education, Science and Technology of Kenya and Kibabii University, Kenya, for providing an opportunity to undertake Ph.D. studies.

**Author contribution** Geoffrey W. Khamala: formal analysis, methodology, visualization, investigation, and writing—original draft. John W. Makokha: conceptualization, resources, supervision, and writing—review and editing. Richard Boiyo: supervision and writing—review and editing. Kanike Raghavendra Kumar: Funding acquisition and writing—review and editing.

**Funding** The author KRK thank the Science and Engineering Research Board (a statutory body of the Department of Science and Technology (DST)), New Delhi, for granting sponsored research project under the Start-up Research Grant (SRG) Scheme of SERB (File No: SRG/2020/001445). One of the authors, KRK, is grateful to the DST, Govt. of India, for the award of the DST-FIST Level-1 (File No. SR/FST/PS-1/2018/35) scheme to the Department of Physics, KLEF, India.

**Data availability** Datasets utilized in the present study can be accessed at the following links: all the optical properties of AOD can be downloaded at http://giovanni.gsfc.nasa.gov/giovanni/.

## Declarations

**Ethics approval and consent to participate** All authors actively participated in processing, writing, editing, and reviewing the manuscript.

**Consent for publication** All the authors agree to the publication of the present manuscript.

**Competing interest** The authors declare no competing interests.

## References


Adesina AJ, Kumar KR, Sivakumar V, Piketh SJ (2016) Inter-comparison and assessment of long-term (2004–2013) multiple satellite aerosol products over two contrasting sites in South Africa. J Atmos Sol Terr Phys 148:82–95. https://doi.org/10.1016/j.jastp.2016.09.001

Akkermans T, Clerbaux N (2020) Narrowband-to-broadband conversions for top-of-atmosphere reflectance from the advanced very high-resolution radiometer (AVHRR). Remote Sens 12:305. https://doi.org/10.3390/rs12020305

Aklesso M, Kumar RK, Bua L, Boiyo R (2018) Analysis of spatial-temporal heterogeneity in remotely sensed aerosol properties observed during 2005–2015 over three countries along the Gulf of Guinea Coast in Southern West Africa. Atmos Environ 182:313–324. https://doi.org/10.1016/j.atmosenv.2018.03.062

Aldabash M, Balcik FB, Glantz P (2020) Validation of MODIS C6.1 and MERRA-2 AOD using AERONET observations: a comparative study over Turkey. Atmosphere 11, 905. https://doi.org/10.3390/atmos11090905

Alpert P, Kaufman YJ, Shayel Y, Tanre D, Da Silva A, Joseph YH (1998) Dust forcing of climate inferred from correlation between dust data and model errors. Nature. 395:367–370

Amiridis V, Balis DS, Kazadzis S, Bais A, Giannakaki E, Papayannis A, Zerefos C (2005) Four-year aerosol observations with a Raman lidar at Thessaloniki, Greece, in the framework of European aerosol Research lidar network (EARLINET). J Geophys Res 110:D21203. https://doi.org/10.1029/2005JD006190

Athar H, Nabeel A, Nadeem, I. And Saeed, F. (2021) Projected changes in the climate of Pakistan using IPCC AR5-based climate models. Theor Appl Climatol 145:567–584. https://doi.org/10.1007/s00704-021-03651-8

Ayugi BO, Wen W, Chepkemoi D (2016) Analysis of spatial and temporal patterns of rainfall variations over Kenya. Journal of Environment and Earth Science ISSN 2224-3216 (Paper) ISSN 2225-0948 (Online) 6(11)

Ayugi B, Tan G, Gnitou GT, Ojara M, Ongoma V (2020) Historical evaluations and simulations of precipitation over East Africa from Rossby Centre regional climate model. Atmos Res 232:104705. https://doi.org/10.1016/j.atmosres.2019.104705

Bennouna YS, Cachorro VE, Toledano C, Berjón A, Prats ND, Fuertes R, Gonzalez Rodrigo R, Torres B, De Frutos AM (2011) Comparison of atmospheric aerosol climatologies over southwestern Spain derived from AERONET and MODIS. Remote Sens Environ 115:1272–1284. https://doi.org/10.1016/j.rse.2011.01.011

Boiyo R, Kumar KR, Zhao T, Bao Y (2017) Climatological analysis of aerosol optical properties over east Africa observed from space-borne sensors during 2001–2015. Atmos Environ 152:298–313. https://doi.org/10.1016/j.atmosenv.2016.12.050

Boiyo RK, Kumar R, Zhao T (2018) Spatial variations and trends in AOD climatology over East Africa during 2002–2016: a comparative study using three satellite data sets. Int J Climatol. https://doi.org/10.1002/joc.5446

Boiyo KR, Kumar KR, Zhao T, Guo J (2019) 10-year record of aerosol optical properties and radiative forcing over three environmentally distinct AERONET sites in Kenya, East Africa. J Geophys Res Atmos. https://doi.org/10.1029/2018JD029

Caroline M, Wainwright AB, John H, Marsham C, David P, Rowell D, Declan L, Finney C, Black E (2021) Future changes in seasonality in East Africa from regional simulations with explicit and parameterized convection. Am Meteorol Soc. https://doi.org/10.1175/JCLI-D-20-0450.1

Charlson RJ, Schwartz SE, Hales JM, Cess RD, Coakley JA, Hansen JE, Hofmann DJ (1992) Climate forcing by anthropogenic aerosols. Science 255:423–430. https://doi.org/10.1126/science.255.5043.423

Che H, Zhang XY, Chen HB, Damiri B, Goloub P, Li ZQ et al (2009) Instrument calibration and aerosol optical depth validation of the China aerosol remote sensing network. J Geophys Res 114:D03206. https://doi.org/10.1029/2008JD011030

Dahutia P, Pathak B, Bhuyan PK (2017) Aerosol's characteristics, trends and their climatic implications over Northeast India and adjoining South Asia. Int J Climatol. https://doi.org/10.1002/joc.5240

De Graaf M, Tilstra LG, Aben I, Stammes P (2010) Satellite observations of the seasonal cycles of absorbing aerosols in Africa related to the monsoon rainfall, 1995-2008. Atmos Environ 44:1274–1283. https://doi.org/10.1016/j.atmosenv.2009.12.038

Deng X, Cao W, Huo Y, Yang G, Yu C, He D, Deng W, Fu W, Ding H, Zhai J, Cheng L, Zhao X (2019) Meteorological conditions during a severe, prolonged regional heavy air pollution episode in eastern China from December 2016 to January 2017. Theor Appl Climatol 135:1105–1122. https://doi.org/10.1007/s00704-018-2426-4

Floutsi AA, Korras-carraca MB, Matsoukas C, Hatzianastassiou N, Biskos G (2016) Climatology and trends of aerosol optical depth over the Mediterranean basin during the last 12 years (2002 – 2014) based on collection 006 MODIS-Aqua data. Sci Total Environ 551–552:292–303. https://doi.org/10.1016/j.scitotenv.2016.01.192

Gatebe CK, Tyson PD, Annegarn HJ, Helas G, Kinyua AM, Piketh SJ (2001) Characterization and transport of aerosols over equatorial eastern Africa. Glob Biogeochem Cycles 15:663e672. https://doi.org/10.1029/2000GB001340

Gebrechorkos SH, Hülsmann S, Bernhofer C (2019) Long-term trends in rainfall and temperature using high-resolution climate datasets in East Africa. Sci Rep 9:11376. https://doi.org/10.1038/s41598-019-47933-8

Gelaro R, McCarty W, Suárez MJ, Todling R (2017) The modern-era retrospective analysis for research and applications, Version 2 (MERRA-2). J Clim 30(14). https://doi.org/10.1175/JCLI-D-16-0758.1

Guillén-Lambea S, Carvalho M, Delgado M, Lazaro A (2021) Sustainable enhancement of district heating and cooling configurations by combining thermal energy storage and life cycle assessment. Clean Techn Environ Policy 23:857–867. https://doi.org/10.1007/s10098-020-01941-9

Hammer S, Martin R, Chi L, Torres O, Manning M, Boys B (2018) Insight into global trends in aerosol composition from 2005 to 2015 inferred from the OMI ultraviolet aerosol index. Atmos Chem Phys 18:8097–8112

Hansen JE, Sato M, Ruedy R (1997) Radiative forcing and climate response. J Geophys Res 102:6831–6864

He Q, Li C, Geng F, Lei Y, Li Y (2012) Study on long-term aerosol distribution over the land of East China using MODIS data. Aerosol Air Qual Res 12:304–319

He Q, Zhang M, Huang B (2016) Spatio-temporal variation and impact factors analysis of satellites-based aerosol optical depth over China from 2002 to 2015. Atmos Environ 129:79–90

Holben BN (1986) Characteristics of maximum-value composite images from temporal AVHRR data. Int J Remote Sens 7:1417–1434

Holben BN, Eck TF, Slutsker I, Tanre D, Buis JP, Setzer A, Vermote E, Reagan JA, Kaufman YJ et al (1998) AERONET-A federated instrument network and data archive for aerosol characterization. Remote Sens Environ 66:1–16

Houghton JT, Ding Y, Griggs DJ, Noguer M, Van der Linden PJ, Dac X et al (2013) Intergovernmental panel on climate change (IPCC). Climate change the specific basis. Contribution of working group 1 for the fifth assessment report. Remote Sens Environ 66:1–16

Hsu NC, Tsay SC, King MD, Herman JR (2004) Aerosol properties over bright-reflecting source regions. IEEE Trans Geosci Remote Sens 42:557–569

Hsu NC, Jeong MJ, Bettenhausen C, Sayer AM, Hansell R, Seftor CS, Huang J, Tsay SC (2013) Enhanced Deep Blue aerosol retrieval algorithm: the second generation. J Geophys Res Atmos 118(16):9296–9315. https://doi.org/10.1002/jgrd.50712

Hu K, Kumar KR, Kang N, Boiyo R, Jinwen Wu (2018) Spatiotemporal characteristics of aerosols and their trends over mainland China with the recent Collection 6 MODIS and OMI satellite datasets. Environ Sci Pollut Res 25:6909–6927. https://doi.org/10.1007/s11356-017-0715-6

Ignatov A, Sapper J, Cox S, Laszlo I, Nalli NR, Kidwell KB (2004) Operational aerosol observations (AEROBS) from AVHRR/3 on board NOAA-KLM satellites. J Atmos Ocean Technol 21(1):3–26. https://doi.org/10.1175/1520-0426

Jethva H, Satheesh SK, Srinivasan J, Levy RC (2010) Improved retrieval of aerosol size-resolved properties from moderate resolution imaging spectroradiometer over India: role of aerosol model and surface reflectance. 115(18). https://doi.org/10.1029/2009JD013218

Kang Z, Li Q, Gao XJ, Zhang L, Jia ZX, Feng Y, Qin GS, Qin WP (2014) Gold nanorod saturable absorber for passive mode-locking at 1 μm wavelength. Astro Ltd Laser Physics Letters 11(3):035102

Kang N, Kumar KR, Hu K, Yu X, Yin Y (2016) Long-term (2002–2014) evolution and trend in collection 5.1 level-2 aerosol products derived from the MODIS and MISR sensors over the Chinese Yangtze River Delta. Atmos Res 181:29–43. https://doi.org/10.1016/j.atmosres.2016.06.008

Khan R, Kumar RK, Zhao T, Ali G (2020) The contribution of different aerosol types to direct radiative forcing over distinct environments of Pakistan inferred from the AERONET data. Environ Res Lett 15:114062

Khan R, Kumar KR, Zhao T, Ullah W, de Leeuw G (2021) Interdecadal changes in aerosol optical depth over Pakistan based on the MERRA-2 reanalysis data during 1980–2018. Remote Sens 13:822. https://doi.org/10.3390/rs13040822

Kinney PL, Gatari GM, Volavka-close N, Ngo N, Ndiba PK, Law A, Gachanja A, Gaita MS, Chillrud NS, Sclar E (2011) Traffic impacts on PM2.5 air quality in Nairobi, Kenya. Environ Sci Policy 14:369–378. https://doi.org/10.1016/j.envsci.2011.02.005

Klingmüller K, Pozzer A, Metzger S, Stenchikov GL, Lelieveld J (2016) Aerosol optical depth trend over the Middle East. Atmos Chem Phys 16:5063–5073

Kumar KR, Sivakumar V, Yin Y, Reddy RR, Kang N, Diao Y, Adesina AJ, Yu X (2014) Long-term (2003–2013) climatological trends and variations in aerosol optical parameters retrieved from MODIS over three stations in South Africa. Atmos Environ 95:400–408. https://doi.org/10.1016/j.atmosenv.2014.07.001

Kumar KR, Yin Y, Sivakumar V, Kang N, Yu X, Diao Y, Adesina AJ, Reddy RR (2015) Aerosol climatology and discrimination of aerosol types retrieved from MODIS, MISR and OMI over Durban (29.88◦S, 31.02◦E), South Africa. Atmos Environ 117:9–18. https://doi.org/10.1016/j.atmosenv.2015.06.058

Kumar KR, Kang N, Sivakumar V, Griffith D (2017) Temporal characteristics of columnar aerosol optical properties and radiative forcing (2011-2015) measured at AERONET's Pretoria_CSIR_DPSS site in South Africa. Atmos Environ 165:274–289

Lee KH, Li Z, Wong MS, Xin J, Wang Y, Hao W, Zhao F (2007) Aerosol single scattering albedo estimated across China from a combination of ground and satellite measurements. J Geophys Res 112:D22S15. https://doi.org/10.1029/2007JD009077

Levelt P, Hilsenrath E, Leppelmeier G, van den Oord G, Bhartia P, Tamminen J et al (2006) Science objectives of the ozone monitoring instrument. IEEE Trans Geosci Remote Sens 44(5):1199–1208

Levy RC, Remer LA, Kleidman RG, Mattoo S, Ichoku C, Kahn R, Eck TF (2010) Global evaluation of the collection 5MODIS dark-target aerosol products over land. Atmos Chem Phys 10(21):10399–10420. https://doi.org/10.5194/acp-10-10399-2010

Li J, Carlson B, Dubovik O, Lacis AA (2014) Recent trends in aerosol optical properties derived from AERONET measurements. Atmos Chem Phys 14:12271–12289

Liu Z, Liu Q, Lin HC, Schwartz CS, Lee YH, Wang T (2011) Three-dimensional variational assimilation of MODIS aerosol optical depth: implementation and application to a dust storm over East Asia. J Geophys Res Atmos 116:1–19. https://doi.org/10.1029/2011jd016159

Livingston JM, Redemann J, Russell PB, Torres O, Veihelmann B, Veefkind P, Braak R, Smirnov A, Remer L, Bergstrom RW, Coddington O, Schmidt KS, Pilewskie P, Johnson R, Zhang Q (2009) Comparison of aerosol optical depths from the ozone monitoring instrument (OMI) on aura with results from airborne sunphotometry, other space and ground measurements during MILAGRO/INTEX-B. Atmos Chem Phys Discuss 9:9961–10013

Luo Y, Zheng X, Zhao T, Chen J (2014) A climatology of aerosol optical depth over China from recent 10 years ofMODIS remote sensing data. Int J Climatol 34:863–870. https://doi.org/10.1002/joc.3728

Makokha JW, Angeyo HK (2013) Investigation of radiative characteristics of the Kenyan atmosphere due to aerosols using sun spectrophotometry measurements and the COART Model. Aerosol Air Qual Res 13:201–208

Makokha J, Odhiambo J, Godfrey J (2017) Trend analysis of aerosol optical depth and Angstrom exponent anomaly over East Africa. Atmos Clim Sci 7:588–603. https://doi.org/10.4236/acs.2017.74043

Makokha JW, Odhiambo JO, Shem JG (2018) Long term assessment of aerosol radiative forcing over selected sites of East Africa. J Geosci Environ Prot\ 6:22–34. https://doi.org/10.4236/gep.2018.64002

Mehta M, Singh R, Singh A, Singh N (2016) Recent global aerosol optical depth variations and trends- a comparative study using MODIS and MISR level 3 datasets. Remote Sens Environ 181:137–150

Ngaina J, Muthama J (2014) Monitoring spatial-temporal variability of aerosol over Kenya. Ethiop J Environ Stud Manage 7:244–252. https://doi.org/10.4314/ejesm.v7i3.2

Ngo NS, Gatari M, Yan B, Chillrud SN, Bouhamam K, Kinney PL (2015) Occupational exposure to roadway emissions and inside informal settlements in sub-Saharan Africa: a pilot study in Nairobi, Kenya. Atmos Environ 111:179–184. https://doi.org/10.1016/j.atmosenv.2015.04.008

Nicholson ES (2017) Climate and climatic variability of rainfall over eastern Africa. J Geophys Res - Atmos. https://doi.org/10.1002/2016RG000544

Ongoma V, Chen H (2017) Temporal and spatial variability of temperature and precipitation over East Africa from 1951 to 2010. Meteorol Atmos Phys. https://doi.org/10.1007/s00703-016-0462-0

Pathak B, Bhuyan P (2013) Absorbing and scattering properties of boundary layer aerosols over Dibrugarh, North East India. Int J Remote Sens 35(14). https://doi.org/10.1080/01431161.2014.926424

Prasad AK, Singh RP, Kafatos M, Singh A (2005) Effect of the growing population on the air pollution, climatic variability and hydrological regime of the Ganga Basin, India. In Proceedings of the Symposium S6 Held during the Seventh IAHS Scientific Assembly, Foz do Iguaçu, Brazil, 3–9 April 2005; IAHS Publication: Foz do Iguaçu, Brazil pp 295

Prijith SS, Rao P, Mohan M, Sai M, Ramana M (2017) Trends of absorption, scattering and total aerosol optical depths over India and surrounding oceanic regions from satellite observations: role of local production, transport and atmospheric dnamics. Environ Sci Pollut Res Int

Prospero JM, Ginoux P, Torres O, Nicholson SE, Gill TE (2002) Environmental characterization of global sources of atmospheric soil dust identified with the nimbus 7 total ozone mapping spectrometer (TOMS) absorbing aerosol product. Rev Geophys 40(1):1002. https://doi.org/10.1029/2000RG000095

Ramachandran S, Rupakheti M, Lawrence MG (2020) Aerosol-induced atmospheric Heating rate decreases over South and East Asia as a result of changing content and composition. Nat Res. https://doi.org/10.1038/s41598-020-76936-z

Ramanathan V, Crutzen PJ, Kiehl JT, Rosenfeld D (2001) Aerosols, climate, and the hydrological cycle. Science 294(5549):2119–2124. https://doi.org/10.1126/science.1064034

Remer LA, Kaufman YJ, Tanre D, Matto S, Chu DA, Martins JV et al (2005) The MODIS aerosol algorithm, products, and validation. J Atmos Sci 62(4):947–973. https://doi.org/10.1175/JAS3385.1

Rienecker MM, Suarez JM, Gelaro R, Todling R, Bacmeister J, Liu E, Bosilovich GM, Schubert DS, Takacs L, Kim G, Bloom S, Chen J, Collins D, Conaty A, Dasilva A, Gu W, Joiner J, Koster RD, Lucchesi R et al (2011) MERRA: NASA's modern-era retrospective analysis for research and applications. J Clim 24. https://doi.org/10.1175/JCLI-D-11-00015.1

Satheesh SK, Ramanathan V, Holben BN, Moorthy KK, Loeb NG, Maring H, Prospero JM, Savoie D (2002) Chemical, microphysical, and radiative effects of Indian Ocean aerosols. J Geophys Res 107(D23):4725. https://doi.org/10.1029/2002jd002463

Sayer AM, Hsu NC, Bettenhausen C, Jeong MJ (2013) Validation and uncertainty estimates for MODIS collection 6B Deep Blue aerosol data. J Geophys Res Atmos 118(14):7864–7872. https://doi.org/10.1002/jgrd.50600

Sayer AM, Munchak LA, Hsu NC, Levy RC, Bettenhausen C, Jeong MJ (2014) MODIS Collection 6 aerosol products: comparison between aqua's Deep Blue, dark target, and B merged data sets, and usage recommendations. J Geophys Res Atmos 119(24):13965–13989. https://doi.org/10.1002/2014JD022453

Seinfeld JH, Pandis SN (1998) Atmospheric chemistry and physics from air pollution to climate change. John Wiley and Sons, New York

Stenge M, Stapelberg S, Sus O, Finkensieper S, Würzler B, Philipp D, Hollmann R, Poulsen C, Christensen M, McGarragh G (2020) Cloud reflectance from advanced very high-resolution radiometer post meridiem (AVHRR-PM) dataset version 3: 35-year climatology of global cloud and radiation properties. Earth Syst Sci Data 12:41–60. https://doi.org/10.5194/essd-12-41-2020

Tang R, Lu Q, Guo S, Wang H, Song K, Yu Y, Tan R, Liu K, Shen R, Chen S, Zeng L, Jorga SD, Zhang Z, Zhang W, Shuai S, Robinson AL (2021) Measurement report: distinct emissions and volatility distribution of intermediate-volatility organic compounds from on-road Chinese gasoline vehicles: implication of high secondary organic aerosol formation potential. Atmos Chem Phys 21:2569–2583. https://doi.org/10.5194/acp-21-2569-2021

Tanre D, Kaufman YJ, Herman M, Mattoo S (1997) Remote sensing of aerosol properties over oceans using the MODIS/EOS spectral radiances. J Geophys Res 102(D14):16971–16986. https://doi.org/10.1029/96JD03437

Tegen I, Hollrig P, Chin M, Fung I, Jacob D, Joyce PJ (1997) Contribution of different aerosol species to the global aerosol extinction optical thickness: estimates from model results. J Geophys Res 102:23,895–23,915

Torres O, Bhartia P, Herman J, Ahmad Z, Gleson J (1998) Derivation of aerosol properties from satellite measurements of backscattered ultraviolet radiation: theoretical basis. J Geophys Res 103(D14):17099e17110

Torres O, Bhartia PK, Sinyuk A, Welton EJ, Holben B (2005) Total ozone mapping spectrometer measurements of aerosol absorption from space: comparison to SAFARI 2000 ground-based observations. J Geophys Res 110:D10S18. https://doi.org/10.1029/2004JD004611

Torres O, Tanskanen A, Veihelmann B, Ahn C, Braak R, Bhartia PK et al (2007) Aerosols and surface UV products from ozone monitoring instrument observations: an overview. J Geophys Res 112:D24S47. https://doi.org/10.1029/2007JD008809

Wang Y, Gu X, Li J, Mi XA (2021) Dual-channel aerosol optical depth retrieval algorithm incorporating the BRDF effect from AVHRR over Eastern Asia. Remote Sens 13:365. https://doi.org/10.3390/rs13030365

Weatherhead EC, Reinsel GC, Tiao GC, Meng XL, Choi D, Cheang WK, Keller T, DeLuisi J, Wuebbles DJ, Kerr JB, Miller AJ, Oltmans SJ, Frederick JE (1998) Factors affecting the detection of trends: statistical considerations and applications to environmental data. J Geophys Res 103(D14):17149–17161. https://doi.org/10.1029/98JD00995

Weber M, Coldewey-Egbers M, Fioletov VE, Frith SM, Wild JD, Burrows JP, Long CS, Loyola D (2018) Total ozone trends from 1979 to 2016 derived from five merged observational datasets – the emergence into ozone recovery. Atmos Chem Phys 18:2097–2117. https://doi.org/10.5194/acp-18-2097-2018

Welton EJ, Campbell JR (2002) Micropulse lidar signals: uncertainty analysis. J Atmos Ocean Technol 19:2089–2094. https://doi.org/10.1175/1520-0426(2002)019<2089:MLSUA>2.0

Wu WS, Purser RJ, Parrish DF (2002) Three-dimensional variational analysis with spatially inhomogeneous covariances. Mon Weather Rev 130:2905–2916

Yusuf N, Said RS, Tilmes S, Gbobaniyi E (2021) Multi-year analysis of aerosol optical properties at various timescales using AERONET data in tropical West Africa. J Aerosol Sci 151(2021):105625

Zhang J, Reid JS (2010) A decadal regional and global trend analysis of the aerosol optical depth using a data-assimilation grade over-water MODIS and Level 2 MISR aerosol products. Atmos Chem Phys 10:10949–10963